Extremely Miniaturized Free-Space Measurement System for RF Metamaterial Composite Based on Beam Focusing Transmitarray

Seungwoo Bang, *Graduate Student Member, IEEE*, Taeyeong Yoon, *Graduate Student Member, IEEE*, Byeongjin Kim, *Graduate Student Member, IEEE*, Jaecheol Oh, *Graduate Student Member, IEEE*, Hogyeom Kim, *Graduate Student Member, IEEE*, and Jungsuek Oh, *Senior Member, IEEE*

***Abstract*—This letter proposes a near-field beam focusing transmitarray-based (TA-based) free space measurement system that is extremely miniaturized rather than horn-to-horn and dielectric lens-based measurement systems for radio frequency (RF) metamaterial composites. Reducing the size of the measurement setup is limited due to the natural phenomenon of conventional systems. Contrastively, TA-based system could overcome the limitation because of its phase-shifting ability to maintain the planar appearance. A device-under-test (DUT) was measured without any distortion utilizing the beam focusing characteristic of the proposed TA, which produces a uniform wavefront phase without diffraction over the DUT aperture. The proposed TA could focus the electromagnetic wave within a distance of 2 cm from the horn antenna while maintaining the phase error under 14.5°, resulting in a plane wave-like phase. Consequently, the RF metamaterial composites could be measured at a short focal distance of 21.7% of the distance required by the conventional free-space system without additional absorbers. Further, the frequency response of DUT (i.e., $|S_{21}|$ and $\angle S_{21}$) could be obtained adequately compared with the full-wave simulation. The difference of transmission zero frequency between simulation and measurement was less than 1.6%.**

***Index Terms*—Beam focusing, frequency selective surfaces, measurement systems, metamaterial composites, transmitarray (TA).**

I. Introduction

FOR several decades, metasurfaces adopting metamaterial composites have received attention due to their ability to metamorphose electromagnetic (EM) waves in the spatial domain that are not usually observed in nature [1], [2], [3], [4], [5]. These abilities include not only selecting the frequency of the propagating signal (i.e., conventional bandpass filter), but also converting the polarization of fields, refracting the direction of the propagating waves, absorbing unnecessary signals, and focusing the radiation beam on a specific area [4], [5], [6], [7], [8], [9], [10], [11], [12], [13], [14], [15], [16], [17], [18]. These characteristics play a crucial role in a wide range of EM scenarios, thus facilitating the use of metasurfaces in various radio frequency (RF) applications, such as radomes, reconfigurable intelligent surfaces, and satellite communication [19], [20], [21], [22].

With the growing requirement for metasurface-based applications, there has been a surge in the need for accurate measurement systems to guarantee efficiency of the applications produced. To meet these requirements, various types of systems have been implemented over several decades, such as waveguide-based, horn-to-horn free-space method, and spot-focusing measurement using a dielectric lens [23], [24], [25], [26], [27], [28], [29], [30], [31], [32]. However, measurement systems based on waveguides have difficulties exciting normally incident EM waves because of their non-transverse electromagnetic (TEM) characteristic [23]. This characteristic can generate unwanted higher modes that distort the characterization results in the case of inhomogeneous materials. Furthermore, the device-under-test (DUT) inside the waveguide cross-section must be etched precisely to achieve reliable measurements. Otherwise, an unnecessary air gap may form between the waveguide cross-sections and an accurate response may not be obtained through the measurement system.

The horn-to-horn free-space measurement system is a non-invasive method for characterizing metamaterial composites, which excites the normally incident wave on the DUT aperture. However, a horn-to-horn system should satisfy the far-field distance between the DUT and transmitting and receiving antennas. In this system, the absorbers must be attached around the DUT because the far-field distance between the antennas and DUT induces diffraction, which distorts the frequency response of the DUT. These requirements, including the far-field distance and absorbers, result in bulky measurement systems, making it challenging to construct a compact system [see upper side of Fig. 1(a)].

To minimize the measurement setup, spot-focused free-space measurement systems consisting of a dielectric lens placed over horn antennas have been investigated [28], [29], [30], [31], [32]. Nevertheless, this lens antenna still has difficulty

Manuscript received 15 January 2024; revised 12 February 2024; accepted 13 February 2024. Date of publication 20 February 2024; date of current version 4 June 2024. This work was supported in part by the Samsung Research Funding Center of Samsung Electronics under Grant SRFC-TE2103 (50%) and in part by the Institute of Information and communications Technology Planning and Evaluation (IITP) grant funded by the Korea government (MSIT) through Innovative Fusion Technologies of Intelligent Antenna Material/Structure/Network for THz 6G, (50%), under Grant 2021-0-00763. *(Corresponding author: Jungsuek Oh.)*

Seungwoo Bang, Taeyeong Yoon, Byeongjin Kim, Hogyeom Kim, and Jungsuek Oh are with the Institute of New Media and Communications, Department of Electrical and Computer Engineering, Seoul National University, Seoul 08826, South Korea (e-mail: littlebang97@snu.ac.kr; taeyeong.yoon@snu.ac.kr; anjelcruso@snu.ac.kr; ghrua2424@snu.ac.kr; jungsuek@snu.ac.kr).

Jaecheol Oh is with the Composite Structures and System Department, Korea Institute of Materials Science, Changwon 51508, South Korea (e-mail: jcoh@kims.re.kr).

Digital Object Identifier 10.1109/LAWP.2024.3367497

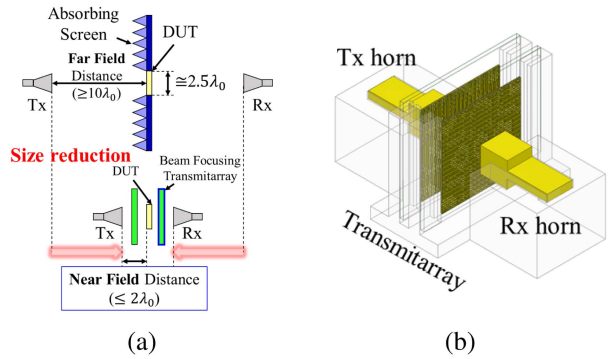

Fig. 1. (a) Miniaturization procedure of the proposed system. (b) Schematic of the proposed measurement system.

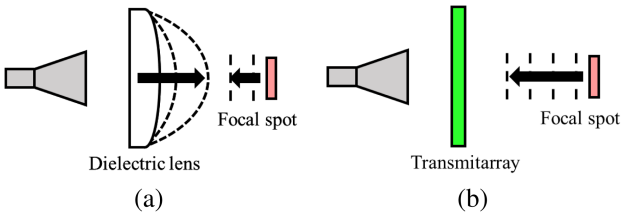

Fig. 2. Measurement appearance compared with (a) dielectric lens-based and (b) proposed beam focusing systems to the focal distance.

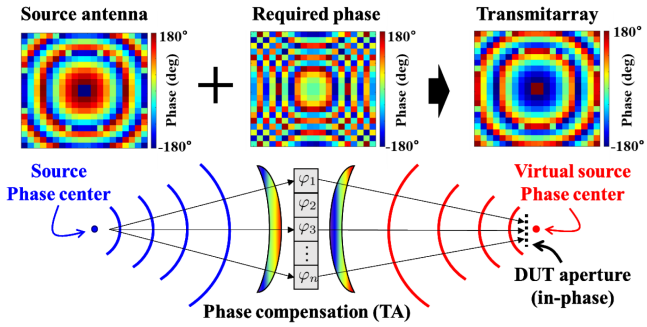

Fig. 3. Wavefront phase of the source antenna, required phase, and TA, respectively.

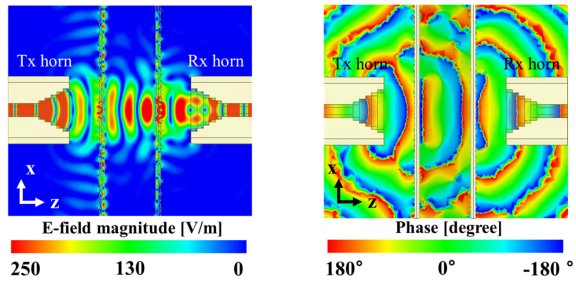

Fig. 4. E-field (a) magnitude and (b) phase distributions of proposed measurement system at 28 GHz (*xz*-plane).

decreasing the focal distance between the antennas and DUT due to its inversely proportional relationship: focal distance and curvature size of the antenna. Fig. 2 depicts the measurement appearance of lens-based spot-focus systems. From the figure, the curvature of the dielectric lens should be large for a short focal distance because the curvature of the lens increases as the compensation for the wavefront phase increases. Moreover, the fabrication process of a dielectric lens is more complex and expensive in proportion to its curvature. Therefore, it is necessary to overcome the limitation of the dielectric lens antennas by implementing a planar structure for achieving a short focal distance.

The approach in this letter starts by constructing planar, noninvasive, and low-cost hardware that overcomes the aforementioned limitations for the miniaturization of a measurement system. Because a transmitarray (TA) antenna satisfies all of the above requirements, this study proposes an extremely miniaturized free-space measurement system based on a beam focusing TA antenna. Fig. 1 shows the schematics of the proposed measurement system. As shown in the figure, the proposed measurement system performs at an extremely short horn-to-horn distance (i.e., less than $4\lambda_0$ at 28 GHz) without additional absorbers around the DUT. The rest of this letter is organized as follows. Section II presents the beam focusing properties of the proposed TA antenna and unit cell designs. In Section III, the fabrication and measurement process of the proposed system is verified. Finally, Section IV concludes this letter.

II. Design Procedure of the Proposed System

A. Near-Field Focusing TA

To focus the beam on an aperture with an arbitrary position and area, this letter compensated for the wavefront of the EM wave through the operating principle of a retrodirective antenna [33].

The transmission phase required for the compensation in the TA is as follows:

$$\varphi_r(x_i, y_j) = \overline{\varphi_{\text{ape}}(x_i, y_j)} - \varphi_{fs}(x_i, y_j) + \varphi_0 \tag{1}$$

where (x_i, y_j) is the position on the TA aperture, φ_r is the phase required for compensation, φ_{fs} is the wavefront phase from the source antenna, and φ_0 is the reference phase. φ_{ape} is the phase of the wavefront propagating to the TA assuming that the EM wave radiates inversely from the arbitrary aperture where the EM wave is focused (i.e., from virtual source in Fig. 3). Fig. 3 shows the wavefront phase distribution of the proposed TA design. Because of the natural phenomenon of the antenna radiation, the wavefront phase from the source antenna(φ_{fs}) has a convex shape to the direction of propagation. To focus the beam on the desired DUT aperture, the proposed design compensates its wavefront(φ_r) into a concave shape through the TA antenna. Fig. 4(a) and (b) depicts the distributions of the electric field intensity and phase radiated from the TA, respectively. These distributions can be the basis for the beam focusing ability of the TA because there is no spillover around the aperture of interest, whereas the phase distribution on the aperture is uniform. Furthermore, the focal distance of the proposed TA should be considered to avoid coupling between the feeder and TA. If they were placed too closely, undesirable errors due to coupling could occur. Fig. 5(a) and (b) shows the magnitude and phase distributions of the focal spot, respectively. Based on Figs. 4 and 5, the 3 dB beamwidth and phase error within the beamwidth, which can affect the frequency responses of the measurement system, were confirmed through full-wave simulation. Table I lists the sizes of the focal spots for several frequencies.

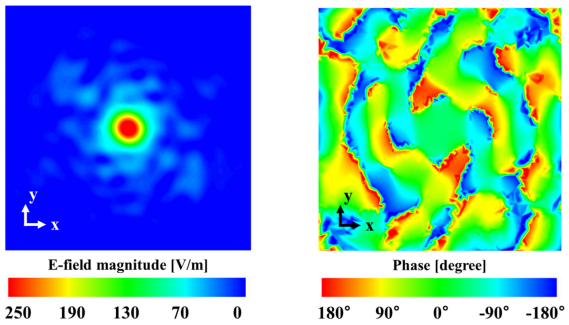

Fig. 5. E-field (a) magnitude and (b) phase distributions of focal spot at 28 GHz (xy-plane). DUT will be placed on the focal spot.

TABLE I
FOCAL SPOT SIZE OF PROPOSED MEASUREMENT SYSTEM

Frequency [GHz]	3 dB beamwidth E-plane	3 dB beamwidth H-plane	Phase error [°]
24	$0.66\lambda_0$	$0.96\lambda_0$	13.1
28	$1.26\lambda_0$	$1.01\lambda_0$	14.5
32	$1.08\lambda_0$	$0.74\lambda_0$	9.1

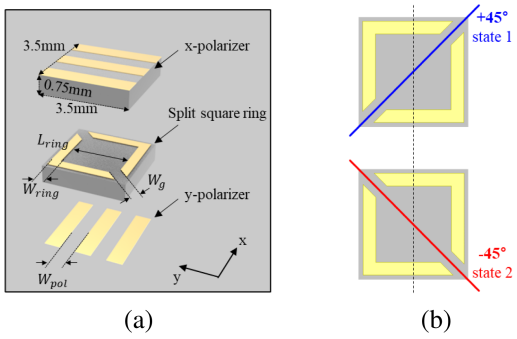

Fig. 6. (a) Exploded view of the proposed unit cell design. (b) States of the proposed unit cell: two states have different phase of 180° since the direction of the E-field excited reversely.

According to Table I, the phase error on the DUT aperture is under 22.5°, which is considered a plane wave condition [34]. Further, it is noticed that samples of size $1.26\lambda_0 \times 1.01\lambda_0$ or larger can be precisely measured at a horn-to-horn distance of 4 cm under the frequency range of 24–32 GHz. This distance is reduced to 21.7% of the far-field distance of the horn antenna without the TA, which is required by the conventional free space measurement system.

B. Unit Cell Design

Fig. 6(a) shows the exploded view of the proposed unit cell design. The unit cell was selected as a polarization rotating unit cell with properties of wideband, via-less, and easy fabrication [7], [35], [36]. The Taconic-TLY5 substrates ($\varepsilon_r = 2.2$ and $\tan\delta = 0.003$) with a thickness of 0.75 mm were placed between the copper layers. The period of the unit cell was 3.5 mm. The split square-ring structure among the polarizers

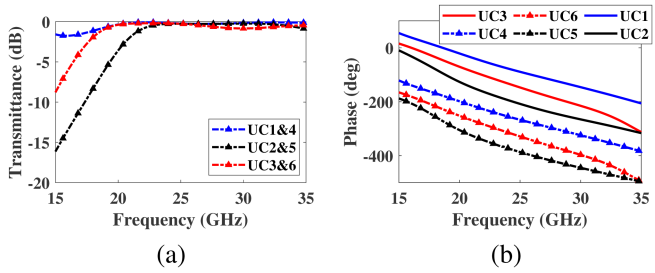

Fig. 7. Frequency responses of the proposed unit cell design: (a) Transmittance. (b) Phase delay.

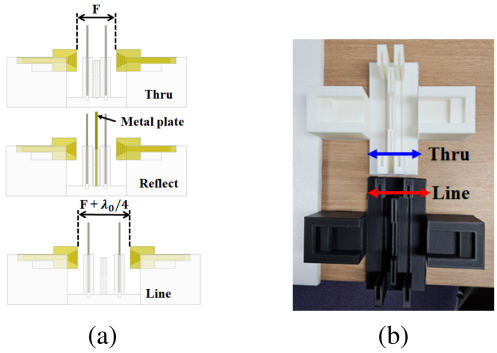

Fig. 8. (a) TRL calibration schematics of the proposed measurement system. (b) 3-D-printed jig for TRL calibration.

converts the polarization of the incident waves. If the split square ring is placed in the reversed direction, the transmission phase changes by 180°, while the transmittance still does not change because the direction of the field on the polarizer is excited in opposite directions [see Fig. 6(b)]. Therefore, it is noticeable that the proposed unit cell could expand the phase tuning range by minimizing the resonant frequency variance to overcome the bandwidth limitation. Fig. 7(a) and (b) shows the amplitudes and phases of the wave transmitted through the proposed unit cell, respectively. As mentioned previously, unit cell pairs that have the same dimensions but different directions of the split square ring (e.g., UC1&4, UC2&5, and UC3&6) show the same amplitude and a phase difference of 180° among the operating frequencies. The proposed unit cells achieved a phase range of 360° and a 1 dB bandwidth of 42% at frequency ranging from 22.5 to 34.7 GHz.

III. FABRICATION AND MEASUREMENT

The proposed measurement system utilizes the through-reflect-line (TRL) calibration technique with time gating to reduce inaccuracies from the measurement system, which also minimizes the reflection and loss within the unit cell [28]. Fig. 8(a) depicts the schematic configuration of the TRL calibration in free space. The through standard can be implemented by placing the TA antennas facing each other at a focal distance. At the same distance, the reflect standard can be realized by placing a metal plate in the space of the DUT. Finally, the line standard can be implemented by increasing the distance between the TAs by a quarter wavelength. Fig. 8(b) shows the jigs fabricated for

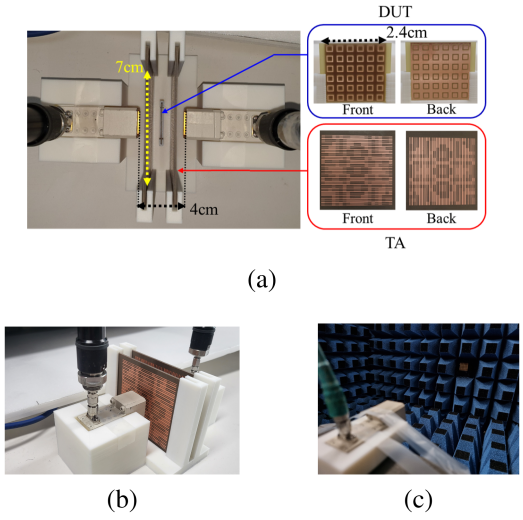

Fig. 9. (a) Top view of the measurement system and proposed DUT and TA samples. (b) Measurement setup with focusing TA. (c) Measurement setup of horn-to-horn free-space system.

TABLE II
UNIT CELL GEOMETRY

Cell #	State	W_{pol}	W_{ring}	W_g	L_{ring}
UC1/4	1/2	0.7mm	0.5mm	0.4mm	1.1mm
UC2/5	1/2	1mm	0.4mm	0.3mm	0.9mm
UC3/6	1/2	0.4mm	0.4mm	0.3mm	1.3mm

TRL calibration of the system. The 3D-printed jigs have different lengths owing to the different distances between the TAs.

Fig. 9(a) presents the top view of the measurement system and the fabricated DUT and beam focusing TA pairs. Ka-band horn pairs are connected to a vector network analyzer. The TA pairs are fabricated with an aperture of 70 mm $\times$ 70 mm (i.e., 20 $\times$ 20 elements). The size of TAs is designed to maintain spillover efficiency over 90% across all operating frequencies. The geometries of the selected unit cells are described in Table II, and the unit cells are located according to (1). Different geometries of the unit cells shift the center frequencies of the unit cells. Therefore, unit cells satisfy the required phase delay for phase compensation [35].

To verify the proposed system, a ring-resonator-based complementary frequency selective surface (CFSS) is employed as a reference. Owing to the equivalent circuit responses of the CFSS, the series *LC*, and parallel *LC* resonators are connected in parallel on a transmission line, so one transmission zero and one transmission pole can exist among the operation frequencies under the proposed system [25]. The transmission zero and pole of the DUT are located at 25.5 and 32 GHz, respectively. The resonator was fabricated using an FR-4 substrate with a period of 4 mm, and an aperture size of 24 mm $\times$ 24 mm.

For validating process, the transmission coefficient and phase delay (i.e., $|S_{21}|$ and $\angle S_{21}$) of the reference DUT are measured and compared with the proposed measurement system and conventional horn-to-horn free-space system [see Fig. 9(b) and (c)]. As shown in Fig. 10(a) and (b), the measurement results are acceptable when compared with those of the full-wave simulation. The measured transmission zero of the DUT is located

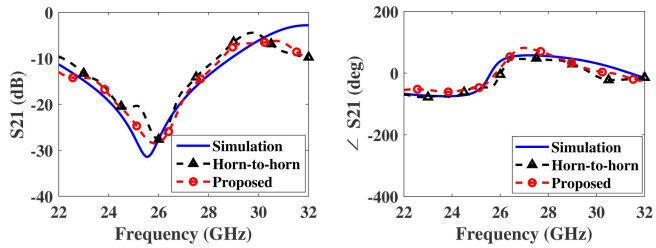

Fig. 10. Frequency responses of the measurement system compared to simulation and measurement. (a) Magnitude. (b) Phase.

TABLE III
COMPARISON TABLE

Ref. #	Freq. (f_0)	Diameter @ f_0	Focal distance* @ f_0	3 dB beamwidth (E-/H-plane)
[28]	16 GHz	$16.3\lambda_0$	$16.3\lambda_0$	N.A.
[29]	30 GHz	$7.8\lambda_0$	$18\lambda_0$	$2.2\lambda_0/2.2\lambda_0$
[30]	10 GHz	$10.2\lambda_0$	$10.2\lambda_0$	$1.07\lambda_0/1.46\lambda_0$
[31]	272.5 GHz	N.A.	$318.2\lambda_0$	$\leq 18.2\lambda_0$
[32]	10.2 GHz	N.A.	$13.6\lambda_0$	$\leq 17\lambda_0$
[37]	26.8 GHz	$9\lambda_0$	$20\lambda_0$	$2.4\lambda_0/2.4\lambda_0$
Proposed	28 GHz	$6.5\lambda_0$	$1.9\lambda_0$	$1.26\lambda_0/1.01\lambda_0$

* Distance between the antenna and the DUT sample.

at 25.9 GHz. The accurate responses with simulation are shown not only in the $|S_{21}|$ but also in the $\angle S_{21}$; thus, the results can be considered reliable. Table III is the comparison table between the measurement system adopting dielectric lens antennas and the proposed system. The remarkable point of view is the physical size of the proposed one, which is relatively miniaturized to conventional systems.

IV. CONCLUSION

This letter presents an extremely miniaturized free-space measurement system based on a beam focusing TA suitable for RF metamaterial composites. The TA can achieve a short focal distance, unlike traditional dielectric lens antennas, owing to its planar structure. This characteristic is noticed because traditional systems have limitations for miniaturizing due to their natural feature (e.g., requiring far-field distance or curvature appearance.). The distance between the Tx and Rx horn antennas was reduced to 21.7% of that required by the conventional free-space system at 28 GHz. A retrodirective antenna-based unit cell arrangement is presented, and its ability to focus EM waves by providing a uniform wavefront phase on the focal spot is demonstrated. Spot-focused TA was implemented using a low-cost PCB manufacturing process that is easy to fabricate. The reliability of the proposed system was validated by measuring a known sample. The measured result of the transmittance and phase delay matched with the full-wave simulation. Therefore, the proposed system can substitute traditional large-scale and sensitive systems such as waveguide-based, horn-to-horn free-space method, and dielectric lens-based spot-focused measurement systems.

REFERENCES

[1] J. B. Pendry, D. Schurig, and D. R. Smith, "Controlling electromagnetic fields," *Science*, vol. 312, no. 5781, pp. 1780–1782, 2006.

[2] D. R. Smith, W. J. Padilla, D. Vier, S. C. Nemat-Nasser, and S. Schultz, "Composite medium with simultaneously negative permeability and permittivity," *Phys. Rev. Lett.*, vol. 84, no. 18, 2000, Art. no. 4184.

[3] D. Schurig, J. Mock, and D. Smith, "Electric-field-coupled resonators for negative permittivity metamaterials," *Appl. Phys. Lett.*, vol. 88, no. 4, 2006, Art. no. 041109.

[4] T.-K. Wu, "Frequency selective surfaces," *Encyclopedia RF Microw. Eng.*, 2005, doi: 10.1002/0471654507.eme133.

[5] K. Sarabandi and N. Behdad, "A frequency selective surface with miniaturized elements," *IEEE Trans. Antennas Propag.*, vol. 55, no. 5, pp. 1239–1245, May 2007.

[6] H. Zhu, S. Cheung, K. L. Chung, and T. I. Yuk, "Linear-to-circular polarization conversion using metasurface," *IEEE Trans. Antennas Propag.*, vol. 61, no. 9, pp. 4615–4623, Sep. 2013.

[7] Z. Liu, H. Niu, Y. Lei, B. Zhao, and L. Zhao, "Design of broadband transmission polarization conversion metasurface based on cross-shaped resonators," *Appl. Phys. A*, vol. 128, no. 8, 2022, Art. no. 681.

[8] J. Oh, "Millimeter-wave thin lens employing mixed-order elliptic filter arrays," *IEEE Trans. Antennas Propag.*, vol. 64, no. 7, pp. 3222–3227, Jul. 2016.

[9] D. Seo, H. Kim, S. Oh, J. Kim, and J. Oh, "Ultrathin high-gain D-band transmitarray based on a spatial filter topology utilizing bonding layer effect," *IEEE Antennas Wireless Propag. Lett.*, vol. 21, no. 10, pp. 1945–1949, Oct. 2022.

[10] S. Hong, Y. Kim, and J. Oh, "Automobile laminated glass window embedded transmitarray and ray tracing validation for enhanced 5G connectivity," *IEEE Trans. Antennas Propag.*, vol. 70, no. 8, pp. 6671–6682, Aug. 2022.

[11] S. Chang, Y. Youn, D. Lee, D. Kim, K. Kweon, and W. Hong, "Method of designing a planar scan angle enhancing meta lens featuring lossless wide scanning at mmWave," *IEEE Trans. Antennas Propag.*, vol. 71, no. 1, pp. 433–442, Jan. 2023.

[12] G. Kim, M. Hwang, I. Lee, and S. Kim, "Design and verification of a miniaturized multifunctional transmitarray unit cell for the S-band," *J. Electromagn. Eng. Sci.*, vol. 23, no. 6, pp. 502–511, 2023.

[13] M. Lyou, G. Kim, and B. Lee, "Design of thin and wideband microwave absorbers using general closed-form solutions," *J. Electromagn. Eng. Sci.*, vol. 21, no. 5, pp. 430–438, 2021.

[14] D. Lim and S. Lim, "Ultrawideband electromagnetic absorber using sandwiched broadband metasurfaces," *IEEE Antennas Wireless Propag. Lett.*, vol. 18, no. 9, pp. 1887–1891, Sep. 2019.

[15] Y. Youn, A. A. Omar, D. Kim, S. Chang, and W. Hong, "Low-profile wideband D-band absorber utilizing resistive thin film screen-printing," *IEEE Trans. Compon., Packag. Manuf. Technol.*, vol. 13, no. 4, pp. 580–582, Apr. 2023.

[16] C.-H. Lee and J.-H. Lee, "Non-uniform amplitude transmitarray for multi-beam including near-field focusing," *IEEE Trans. Antennas Propag.*, vol. 71, no. 1, pp. 361–367, Jan. 2023.

[17] Y. Youn, D. Kim, S. Chang, J. Choi, and W. Hong, "Scattering mitigation frequency selective surface for unidirectional blockage compensation," *IEEE Trans. Antennas Propag.*, vol. 70, no. 12, pp. 12387–12392, Dec. 2022.

[18] A. H. Abdelrahman, A. Z. Elsherbeni, and F. Yang, "High-gain and broadband transmitarray antenna using triple-layer spiral dipole elements," *IEEE Antennas Wireless Propag. Lett.*, vol. 13, pp. 1288–1291, 2014.

[19] F. Costa and A. Monorchio, "A frequency selective radome with wideband absorbing properties," *IEEE Trans. Antennas Propag.*, vol. 60, no. 6, pp. 2740–2747, Jun. 2012.

[20] J. Kim, J. Kim, J. H. Oh, S.-H. Wi, and J. Oh, "Rotated feed-combined reconfigurable transmit RIS with disparate deployment of 1-bit hybrid units for B5G/6G," *IEEE Trans. Antennas Propag.*, vol. 71, no. 6, pp. 5457–5462, Jun. 2023.

[21] H.-B. Jung and J.-H. Lee, "Theoretical and experimental investigation of N-bit reconfigurable retrodirective metasurface," *J. Electromagn. Eng. Sci.*, vol. 24, pp. 42–50, 2024.

[22] H. Kim, J. Kim, and J. Oh, "A novel systematic design of high-aperture-efficiency 2D beam-scanning liquid-crystal embedded reflectarray antenna for 6G FR3 and radar applications," *IEEE Trans. Antennas Propag.*, vol. 70, no. 11, pp. 11194–11198, Nov. 2022.

[23] H. Kim, J. Kim, and J. Oh, "Liquid-crystal-based X-band reactively loaded reflectarray unit cell to reduce reflection loss," *IEEE Antennas Wireless Propag. Lett.*, vol. 20, no. 10, pp. 1898–1902, Oct. 2021.

[24] M.-S. Park, J. Cho, S. Lee, Y. Kwon, and K. Y. Jung, "New measurement technique for complex permittivity in millimeter-wave band using simple rectangular waveguide adapters," *J. Electromagn. Eng. Sci.*, vol. 22, no. 6, pp. 616–621, 2022.

[25] C.-K. Lee, S. Zhang, S. S. Bukhari, D. Cadman, J. Vardaxoglou, and W. G. Whittow, "Complex permittivity measurement system for solid materials using complementary frequency selective surfaces," *IEEE Access*, vol. 8, pp. 7628–7640, 2020.

[26] X. Zhou et al., "A novel design of a compact frequency-selective surface with high selectivity and angular stability," *IEEE Microw. Wireless Compon. Lett.*, vol. 32, no. 7, pp. 931–934, Jul. 2022.

[27] G.-W. Chen et al., "High roll-off frequency selective surface with quasi-elliptic bandpass response," *IEEE Trans. Antennas Propag.*, vol. 69, no. 9, pp. 5740–5749, Sep. 2021.

[28] D. K. Ghodgaonkar, V. V. Varadan, and V. K. Varadan, "A free-space method for measurement of dielectric constants and loss tangents at microwave frequencies," *IEEE Trans. Instrum. Meas.*, vol. 38, no. 3, pp. 789–793, Jun. 1989.

[29] N. Gagnon, J. Shaker, P. Berini, L. Roy, and A. Petosa, "Material characterization using a quasi-optical measurement system," *IEEE Trans. Instrum. Meas.*, vol. 52, no. 2, pp. 333–336, Apr. 2003.

[30] D. Ghodgaonkar, V. Varadan, and V. K. Varadan, "Free-space measurement of complex permittivity and complex permeability of magnetic materials at microwave frequencies," *IEEE Trans. Instrum. Meas.*, vol. 39, no. 2, pp. 387–394, Apr. 1990.

[31] S. Kim, D. Novotny, J. A. Gordon, and J. R. Guerrieri, "A free-space measurement method for the low-loss dielectric characterization without prior need for sample thickness data," *IEEE Trans. Antennas Propag.*, vol. 64, no. 9, pp. 3869–3879, Sep. 2016.

[32] U. C. Hasar et al., "Improved method for permittivity determination of dielectric samples by free-space measurements," *IEEE Trans. Instrum. Meas.*, vol. 71, 2022, Art. no. 6002108.

[33] Y. Chang, H. R. Fetterman, I. L. Newberg, and S. K. Panaretos, "Microwave phase conjugation using antenna arrays," *IEEE Trans. Microw. Theory Techn.*, vol. 46, no. 11, pp. 1910–1919, Nov. 1998.

[34] C. A. Balanis, *Antenna Theory: Analysis and Design*. Hoboken, NJ, USA: Wiley, 2016.

[35] K. Mavrakakis, H. Luyen, J. H. Booske, and N. Behdad, "Wideband transmitarrays based on polarization-rotating miniaturized-element frequency selective surfaces," *IEEE Trans. Antennas Propag.*, vol. 68, no. 3, pp. 2128–2137, Mar. 2020.

[36] P.-Y. Feng, S.-W. Qu, and S. Yang, "Octave bandwidth transmitarrays with a flat gain," *IEEE Trans. Antennas Propag.*, vol. 66, no. 10, pp. 5231–5238, Oct. 2018.

[37] Eravant, "Ka-band spot-focusing lens antenna," 2023. Accessed: Mar. 11, 2024. [Online]. Available: https://www.eravant.com